Asian Journal of Pharmaceutical Sciences 18 (2023) 100833

Available online at www.sciencedirect.com

ScienceDirect

journal homepage: www.elsevier.com/locate/AJPS

Original Research Paper

Pulmonary delivery of mucus-traversing PF127-modified silk fibroin nanoparticles loading with quercetin for lung cancer therapy ☆

Yu Tang[a,1], *Lanfang Zhang*[a,1], *Rui Sun*[a], *Baiyi Luo*[a], *Yu Zhou*[a], *Yan Zhang*[a], *Yuqi Liang*[b], *Bo Xiao*[b], *Chenhui Wang*[a,*]

[a] *Chongqing Key Laboratory of Natural Product Synthesis and Drug Research, Innovative Drug Research Center, School of Pharmaceutical Sciences, Chongqing University, Chongqing 401331, China*

[b] *State Key Laboratory of Silkworm Genome Biology, College of Sericulture, Textile and Biomass Sciences, Southwest University, Chongqing 400715, China*

ARTICLE INFO

Article history:
Received 6 October 2022
Revised 24 July 2023
Accepted 26 July 2023
Available online 28 July 2023

Keywords:
Pulmonary drug delivery
Mucus penetration
Quercetin
Pluronic F127

ABSTRACT

The mucosal barrier remains a major barrier in the pulmonary drug delivery system, as mucociliary clearance in the airway accelerates the removal of inhaled nanoparticles (NPs). Herein, we designed and developed the inhalable Pluronic F127-modified silk fibroin NPs loading with quercetin (marked as QR-SF (PF127) NPs), aiming to solve the airway mucus barrier and improve the cancer therapeutic effect of QR. The PF127 coating on the SF NPs could attenuate the interaction between NPs and mucin proteins, thus facilitating the diffusion of SF(PF127) NPs in the mucus layer. The QR-SF (PF127) NPs had particle sizes of approximately 200 nm with negatively charged surfaces and showed constant drug release properties. Fluorescence recovery after photobleaching (FRAP) assay and transepithelial transport test showed that QR-SF (PF127) NPs exhibited superior mucus-penetrating ability in artificial mucus and monolayer Calu-3 cell model. Notably, a large amount of QR-SF (PF127) NPs distributed uniformly in the mice airway section, indicating the good retention of NPs in the respiratory tract. The mice melanoma lung metastasis model was established, and the therapeutic effect of QR-SF (PF127) NPs was significantly improved *in vivo*. PF127-modified SF NPs may be a promising strategy to attenuate the interaction with mucin proteins and enhance mucus penetration efficiency in the pulmonary drug delivery system.

☆ Peer review under responsibility of Shenyang Pharmaceutical University.

* Corresponding author.
E-mail address: wangchenhui@cqu.edu.cn (C. Wang).

[1] These authors contributed equally to this work.
Peer review under responsibility of Shenyang Pharmaceutical University.

https://doi.org/10.1016/j.ajps.2023.100833

1. Introduction

Lung cancer is the principal cause of cancer death worldwide. According to the differentiated stages and morphological characteristics, lung cancers are typically divided into non-small cell lung cancers (NSCLC) and small cell lung cancers (SCLC) [1–3]. NSCLC has attracted growing attention due to its high incidence and poor survival. Thus far, chemotherapy has been extensively used for the treatment of NSCLC, but the nonspecific distribution and concomitant systemic toxic side effects limit the therapeutic effect [4–6]. It appeared that the pulmonary drug delivery system would be a more suitable lung cancer treatment option, as it can increase the drug concentration in the lesion site and minimize the systemic side effects [7–9].

Inorganic nanomaterials-based nanocarriers have been utilized as efficient pulmonary drug delivery system for their ease of preparation, homogeneity and multi-functionality [10,11]. However, the toxicity to the lung tissues restricts the pulmonary application of inorganic nanocarriers [12,13]. Therefore, biodegradable and biocompatible materials gathered tremendous attention. Phospholipid-based nanocarriers, such as solid lipid nanoparticles (SLNs), liposomes and lipid nanocapsules (LNCs), have been widely employed in inhaled administration because of their high cell affinity and excellent cell uptake [14–16]. Additionally, biodegradable polymers such as poly (lactic-*co*-glycolic) acid (PLGA) and poly (*L*-lactic acid) (PLLA) have been processed into NPs and used as pulmonary drug delivery carriers due to their structural integrity, physical stability and controlled release property [17–19]. However, the acidic degradation products of polymers can evoke immunological responses, which potentially risk human health safety, largely impeding their further application in pulmonary drug delivery [20,21]. Considering the drawbacks of synthesized polymers, natural polymers have been proposed as a promising replacement used in pulmonary drug delivery. Silk fibroin (SF), a natural protein extracted from silkworm cocoons containing heavy and light chains linked by a disulfide bond, has been an ideal material in drug delivery systems for their intrinsic degradability, low immunogenicity, good mechanical property and excellent biocompatibility [22–26]. Importantly, it has already been approved by the US Food and Drug Administration (FDA) as a biological material [27]. Yang et al. prepared doxorubicin-loaded magnetic SF nanoparticals (NPs), which served as novel drug delivery system (NDDS) for multidrug-resistant cancer treatment [28]. With respect to the application in pulmonary drug delivery, Wu et al. designed the inhalable ciprofloxacin hydrochloride microparticles (CMs) using SF and mannitol for the treatment of non-cystic fibrosis bronchiectasis (NCFB), proving that SF might be a promising material in pulmonary drug delivery [29].

Nevertheless, the pulmonary drug delivery system is often greatly hurdled by the body's natural defense mechanism of the viscous mucus layer and mucociliary clearance [30]. Mucus is viscoelastic hydrogel secreted by goblet epithelial cells, consisting of a crosslinked network of negatively charged mucin monomers, covering the surface of the respiratory tract [31–36]. Inhaled NPs can be trapped by mucus through a variety of physicochemical interactions such as hydrophobic interactions, electrostatic interactions and Van der Waals interactions, and then be rapidly eliminated by mucociliary clearance and eventually swallowed or coughed up [37–39]. Considering mucociliary clearance seriously affects the intratracheal and pulmonary delivery efficiency, NPs with mucus-penetrating ability are essential to successful pulmonary delivery. It has been reported that Pluronic F127 (PF127), a copolymer approved by the FDA, was effective in attenuating the interaction between NPs and mucin proteins in the crosslinked network. To date, PF127 has been used to conquer the intestinal mucus barrier and improve the efficacy of oral NPs [40–44]. Considering the similar properties of intestinal mucus barrier and airway mucus barrier [45,46], the surface modification of NPs with PF127 is expected to promote the airway mucus permeation performance, and enhance the pulmonary delivery efficiency [37,41,47].

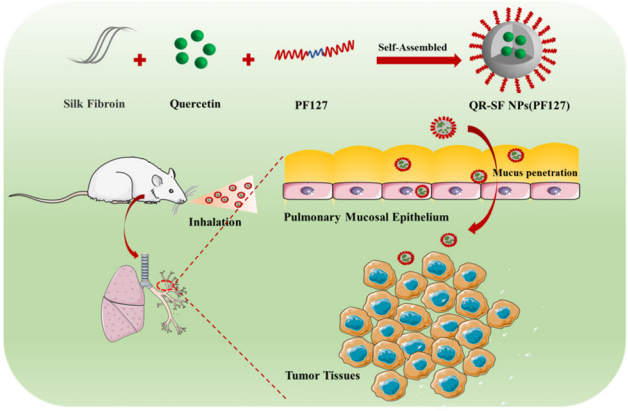

Scheme 1 – Schematic diagram of mucus-traversing PF127-modified silk fibroin nanoparticles loading with quercetin for lung cancer therapy.

Quercetin (QR), a common natural flavonoid, can regulate various intracellular signaling pathways in cancer and has been shown to suppress various cancer cell proliferation [48–50]. But poor water solubility, low bioavailability and systemic distribution of QR greatly hinder its medical applications. Herein, we designed and developed the inhalable PF127-modified SF NPs loading with QR (QR-SF (PF127) NPs), aiming to solve the airway mucus barrier and improve the therapeutic effect of QR. FRAP assay and transepithelial transport test were conducted to validate the mucus-penetrating ability of QR-SF (PF127) NPs. Besides, mice airway sections were obtained to examine the distribution and retention in the respiratory tract. Ultimately, the mice melanoma lung metastasis model was established to evaluate the therapeutic effect. The results show that PF127-modified SF NPs may be a promising strategy to attenuate the interaction with mucin proteins and enhance mucus penetration efficiency in the pulmonary drug delivery system (Scheme 1).

2. Materials and methods

2.1. Materials

Silkworm cocoons were provided by the State Key Laboratory of Silkworm Genome Biology, Southwest University (Chongqing, China). PF127 was purchased from Chengdu Kelong Chemical Co., Ltd. (Chengdu, China). QR and mucin were obtained from Sigma-Aldrich (MO, USA). Phalloidin-iFluor-555-labeled wheat germ agglutinin (WGA) was purchased from AAT Bioquest Inc. (Sunnyvale, USA). Coumarin 6 and thiazolyl blue tetrazolium bromide (MTT) were obtained from Aladdin (Shanghai, China). Calf thymus DNA, Tween 80 and Hank's balanced salt solution (HBSS) were purchased from Solarbio Technology Co. (Beijing, China). DAPI, hemotoxylin and eosin (H&E) stain kit and Annexin V-FITC apoptosis assay kit were obtained from the Beyotime Institute of Biotechnology (Shanghai, China). TUNEL apoptosis detection kit and the immunohistochemistry kit were provided by Servicebio Technology Co., Ltd. (Wuhan, China). A549 cells, L02 cells, HUVEC cells, RAW 264.7 cells Calu-3 cells and human pulmonary artery smooth muscle cells (HPASMCs) were purchased from the national infrastructure of cell line resources (Shanghai, China). And Female BALB/c mice aged 6–8 weeks were obtained from Byrness Weil Biotech Ltd (Chongqing, China). All animal experiments were carried out in compliance with the requirements of the National Act on the Use of Experimental Animals (China) and were approved by the Experimental Animal Ethical Committee of Chongqing University.

2.2. Preparation and characterization of NPs

SF was extracted from silkworm cocoons according to previous methods [40]. SF (100 mg) was dissolved in water (10 mg/ml), and different proportions of PF127 powders were added to the RSF solution (weight ratios of PF127 and SF was 0, 1%, 3%, 5%, 8% and 12%). Meanwhile, QR (5 mg) was dissolved in acetone (10%, w/v). The obtained SF/PF127 mixture was added to the QR solution under vortex, the SF/PF127/QR mixture was sonicated at an amplitude of 30% for 60 s, and acetone was evaporated under reduced pressure for 0.5 h. Finally, the resultant NPs were collected, rinsed with ultrapure water, and then freeze-dried. Freeze-dried NPs (SFNPs, SF(PF127)NPs, QR-SFNPs, QR-SF(PF127)NPs) were dispersed in ultrapure water (pH 7.0) and measured with the Multi-angle particle size and high sensitive zeta potential analyzers (Omni, Brookhaven Instrument Corp, USA). The surface morphology of NPs was observed using transmission electron microscopy (TEM, Talos F200S, Thermo Fisher Scientific CDLtd, Czech).

2.3. Drug loading capacity

The drug loading capacity of SFNPs and SF(PF127)NPs were quantitatively analyzed by a UV–vis spectrophotometer (Agilent Cary60, Agilent Technologies Co. Ltd, USA). QR was extracted from the prepared NPs with acetone and measured by the absorbance (374 nm) of supernatant after centrifugation (16,000 g, 10 min). The drug loading (DL) efficiency was measured as follows:

$$\text{DL (\%)} = \frac{\text{Weight of QR in NPs}}{\text{Weight of loaded QR and NPs}} \times 100\%$$

2.4. In vitro drug release from NPs

The released QR from the two formulations, QR-SFNPs and QR-SF(PF127)NPs, was measured using UV–Vis spectrophotometry. The two formulations were re-suspended separately in 1.0 ml phosphate buffer saline (PBS, pH 7.4) with 1% Tween 80 and loaded into preactivated dialysis bags (MW = 8,000). The dialysis bag was then exposed to a 40 ml release medium at 37 °C and shaken at 150 rpm. At predetermined time points, 4 ml the release medium were taken, and fresh PBS was replenished. The withdrawn samples were assayed by UV/vis spectrophotometer (374 nm). Each experiment was repeated three times.

2.5. Mucus penetration of NPs in vitro

The permeability of NPs within artificial mucus and mucin aqueous solution was evaluated by fluorescence recovery after photobleaching (FRAP) study. The artificial mucus was prepared by emulsifying 250 mg mucin, 110 mg potassium chloride, 250 mg sodium chloride, 100 mg DNA, 0.295 mg DTPA, 1 ml RPMI and 250 µl sterile egg yolk in 50 ml water. Aqueous mucin solution was prepared by dispersing mucin in water (5% w/v) and stirring for 12 h. A centrifuge (3,500 g, 20 min) was used to collect the supernatant. 5 µg fluorescent labeled NPs were mixed separately with 50 µl artificial mucus and mucin aqueous solution. Then the mixture was transferred to the laser confocal petri dish for observation using CLSM (Leica TCS SP8, Leica, Germany). Photobleaching was performed as previously described, and the fluorescence intensity in the circular region was scanned at different time points during fluorescence recovery time.

2.6. Cell viability assay

RAW 264.7 cells, HUVEC cells, L02 cells and HPASMCs were used to analyze the *in vitro* cytotoxic effect of the nanocarriers by standard MTT assay. All four cell lines were plated at a density of 1×10^4 cells per well in 96-well plates and were treated with nanocarriers containing various concentrations. The absorbance was quantified using a plate reader (SpectraMax i3x, Molecular Devices, USA) at 490 nm.

2.7. In vitro cell uptake assay

For the cell uptake experiments, A549 cells were cultured in a 12-well plate (5×10^4 cells/well) and treated with fluorescent-labeled SFNPs, SF(PF127)NPs, or free coumarin 6. After incubation for 1 h at 37 °C, cells were washed,

Table 1 – Particle size, zeta potential and drug loading of NPs. Each value represents the mean ± SD ($n = 3$).

QR-SF(PF127) NPs Formulation	PF127 (%)	Size (nm)	PDI	Zeta potential (mV)	QR loading (%)
NPs-1	0	220.7 ± 2.1	0.15±0.02	−19.6 ± 0.9	5.44±0.146
NPs-2	1	234.2 ± 3.7	0.10±0.03	−19.9 ± 1.2	5.23±0.107
NPs-3	3	237.1 ± 4.1	0.14±0.03	−21.8 ± 0.3	4.79±0.204
NPs-4	5	250.2 ± 2.3	0.11±0.05	−22.8 ± 1.0	4.80±0.125
NPs-5	8	250.2 ± 5.2	0.10±0.05	−24.0 ± 1.0	4.75±0.193
NPs-6	12	284.6 ± 3.1	0.12±0.04	−26.3 ± 1.0	6.12±0.231

fixed, stained and observed with an inverted fluorescence microscope (Leica DMi8, Leica, Germany).

2.8. *Cell apoptosis assay*

Apoptosis-inducing effects of QR-SFNPs and QR-SF(PF127)NPs in A549 cells were evaluated by analytical flow cytometry (CytoFLEX, Beckman Coulter, China) using Annexin V-FITC/PI apoptosis kit. A549 cells were seeded in 12-well plates (5×10^4 cells/well) and incubated with NPs for 24 h. Both early apoptotic and late apoptotic cells were included in cell death determinations.

2.9. *Transepithelial transport of NPs*

Calu-3 cells were grown in the MEM for 1 week, at which point an air-liquid interface (ALI) culture system was initiated using 12-well Corning Transwell® plates (0.4 mm pore size, 1.12 cm^2 surface area). The Calu-3 cell monolayer was established to study the cellular uptake and transepithelial transport of NPs, referring to the method of Liu et al. The transepithelial electrical resistance (TEER) measurement was used to assess the integrity of the cell monolayer. For the cell uptake experiments, the MEM medium in the apical and basolateral compartment was discarded, 0.5 ml HBSS containing coumarin 6-labeled NPs were added to the apical compartment, after incubation for 1 h at 37 °C, cells were washed, fixed and stained as described previously, and observed with CLSM. To observe the interaction between NPs and mucus during transepithelial transport, the Calu-3 cell monolayer was equilibrated with HBSS for 30 min at 37 °C and incubated with coumarin 6-labeled NPs for 6 h. The cell monolayer was washed three times with HBSS and fixed with 4% PFA. The mucus layer was stained with phalloidin-iFluor-555-labeled wheat germ agglutinin and observed with CLSM.

2.10. *Distribution in mouse airway*

Mice were randomly divided into two groups and nebulized with coumarin 6-labeled NPs. The mice were executed 10 min after aerosol inhalation treatment, and the trachea was collected and embedded in OCT. Transverse cryosections were cut at 15 μm using a freezing microtome (Leica CM1950, Leica, Germany). The distribution of NPs in the airway mucus layer in cryosections of the trachea was observed with an inverted fluorescence microscope.

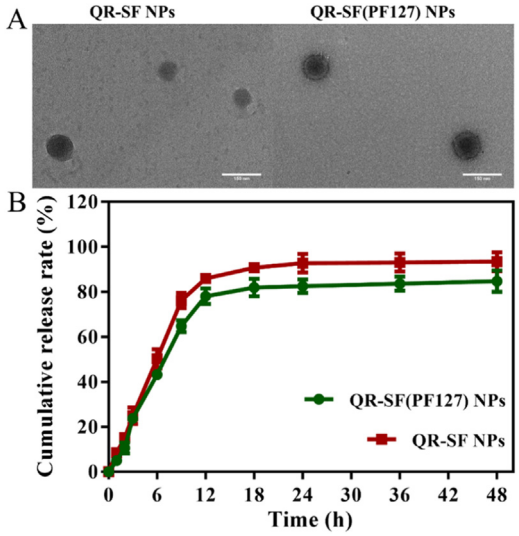

Fig. 1 – (A) TEM images of SF NPs and SF (PF127) NPs loading with QR. (B) *In vitro* QR release profiles of drug-loaded NPs in PBS.

2.11. In vivo *anti-tumor experiments*

The mice model of melanoma lung metastasis was established via lateral tail vein injection (0.1 ml PBS per mouse containing 1×10^6 B16F10 cells). Seven days after tumor implantation, the animals were randomly divided into three groups as follows ($n = 5$), QR-SFNPs and QR-SF(PF127)NPs were given respectively via intratracheal administration to the lungs (QR doses given were 5 mg/kg). The control group was given the same volume of physiological sterile saline. The three mice groups received treatments every 2 d and were sacrificed by dislocating the cervical vertebrae under anesthesia after 14 d treatments. The hearts, livers, spleens, lungs and kidneys of mice were fixed in 4% PFA, and black tumor cell colonies on the surface of lungs were counted. H&E staining was performed to observe morphological changes in the tissues.

2.12. *Histology and apoptosis analysis*

The apoptosis-inducing properties of QR-SFNPs and QR-SF(PF127)NPs *in vivo* were determined by TUNEL analysis. 4% PFA-fixed, paraffin-embedded lung tissues were cut into sections of 3 μm in thickness using a microtome. A TUNEL Apoptosis Kit (Servicebio) was used to detect apoptosis according to the manufacturer's instructions. The microvessels were identified by immunohistological staining for CD31, and the sections were observed with a fluorescence microscope (Leica DM6, Leica, Germany).

2.13. *Statistical analysis*

Data were expressed as the mean value ± SD. Statistical analysis was performed with a one-way analysis of variance (ANOVA) using SPSS software. P value ≤ 0.05 was considered to be statistically significant.

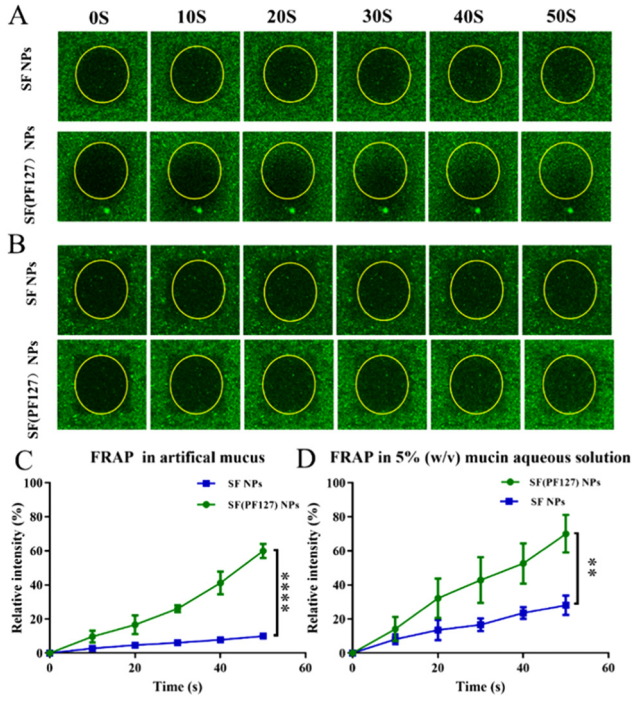

Fig. 2 – (A) Representative images of SF NPs and SF(PF127) NPs at different time points in FRAP study in artificial mucus. (B) Representative images of SF NPs and SF(PF127) NPs at different time points in FRAP study in 5%(w/v) mucin aqueous solution. (C-D) Relative fluorescent intensity of SF NPs and SF(PF127) NPs at different time points during fluorescence recovery. Data are presented as mean ± SD ($n = 3$), $^{**}P < 0.01$, $^{****}P < 0.0001$.

3. Results and discussion

3.1. *Preparation and characterization of NPs*

The particle size of NPs with different weight ratios of PF127 located in a range between 220.7 and 284.6 nm, and the coating of PF127 increases the particle size of NPs (Table 1). It has been reported that the pore size of the mucus in respiratory tract was between 100 and 500 nm. Thus, the NPs with ideal particle size contribute to the rapid mucus penetration of drugs. The drug loading capacity of NPs with different PF127 ratio were in the range of 4.75%–6.12% (Table 1). Overall, the drug loading capacity decreased upon increasing the PF127 ratio which may be caused by the insertion of the PF127 hydrophobic portion. The NPs with 12% PF127 exhibited anomalous drug loading of 6.12%±0.231%, which may be caused by the surface-adhesion by the abundant PF127. The cellular uptake behavior of NPs with different PF127 ratio was shown in Fig. S1. As the PF127 increased from 0 to 5%, the cell uptake was significantly enhanced. But as the level increased to 8%, the cellular uptake decreased. This may be attributable to the interference effect by the excessive PF127 on the surface. The rotating tube assay was employed to evaluate the penetration capacity of NPs with different PF127 ratio. Fig. S1C showed that higher ratio of PF127 offers stronger mucus penetration ability. By comprehensive consideration of particle size, cellular uptake and mucus penetration, SF NPs with 5% PF127 was chosen as the optimal prescription, which was named QR-SF(PF127) NPs. As shown in Fig. 1A, the morphology of QR-SF(PF127) NPs were uniform spherical particles. Notably, the TEM image clearly demonstrated the core-shell structure of QR-SF(PF127) NPs compared with QR-SF NPs. Such morphology discrepancy may be caused by the coating of PF127.The hydrophobic part of PF127 could integrate into SF, while the hydrophilic part of PF127 could bind at the surface of the NPs. Moreover, the particle size of QR-SF(PF127) NPs was slightly larger than that of QR-SF NPs in visual field, which was consistent with the dynamic light scattering results.

3.2. In vitro *drug release and biocompatibility*

Release behaviors of QR from NPs were performed (Fig. 1B). Both QR-SF (PF127) NPs and QR-SF NPs showed a drug release of more than 80% within 24 h. However, QR-SF (PF127) NPs released slightly slower than QR-SF NPs, which might be ascribed to the fact that the coated PF127 retarded the drug release behaviors. MTT assay was performed to investigate the biocompatibility of SF(PF127) NPs. The results are shown in Fig. S2. After incubation for 24 h, all the cell viabilities were greater than 90%, indicating the good biocompatibility and safety of SF(PF127) NPs.

3.3. *Mucus penetration of NPs* in vitro

To achieve successful pulmonary delivery, NPs should be able to readily diffuse through the mucus layer with high efficiency to evade mucociliary clearance. FRAP was employed to observe the translational movement of SF(PF127) NPs in artificial mucus. The extent of the fluorescence intensity increased in the yellow circle during photo recovery was positively associated with the diffusion rates of the NPs. The fluorescence enhancement percentage of SF(PF127) NPs (~60%) was about 5-fold higher than that of SF NPs (~12%) at 50 s in artificial mucus, demonstrating the significantly stronger diffusive capability of SF(PF127) NPs. The increased diffusion rate of SF(PF127) NPs may be due to the fact that PF127 could prevent the adsorption of mucin in artificial mucus (Fig. 2A and 2C). To prove this hypothesis, the FRAP assay in the 5% mucin aqueous solution (w/v) was explored. About 70% of fluorescence recovery was shown in SF(PF127) NPs group at 50 s. In marked contrast, a dramatically lower fluorescence recovery (~20%) appeared in the SF NPs group (Fig. 2B and 2D). Collectively, these results confirm that the PF127 coating on the SF NPs reduced the adhesion of mucin, which thus facilitated the diffusion of SF(PF127) NPs in the mucus layer.

3.4. *Transport ability across the lung epithelium mucus layer*

The transport ability of NPs across the epithelium layer of the lungs was evaluated by Calu-3 cell monolayer model in the transwell plate. Calu-3 cells expressed an intact mucus layer after a 14-d culture. As shown in Fig. 3A, the red,

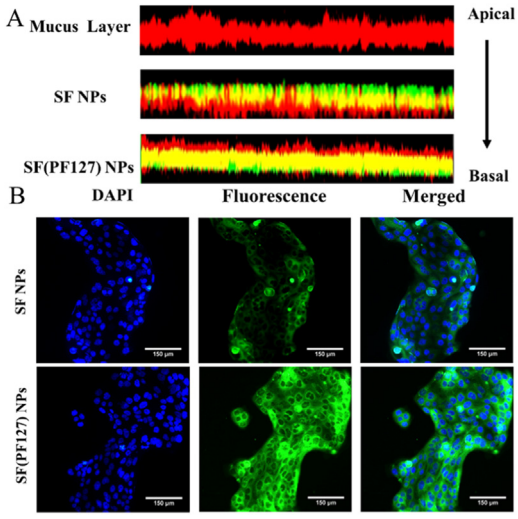

Fig. 3 – (A) The transport ability of NPs across the epithelium layer was evaluated by CLSM in the transwell plate. The red, green and yellow fluorescence represent the mucus, the Coumarin 6-labeled NPs and the colocalization of mucus and NPs, respectively. (B) CLSM images of cellular uptake of NPs in Calu-3 cells. Scale bar =150 μm.

green and yellow fluorescence represent the mucus, the Coumarin 6-labeled NPs, and the colocalization of mucus and NPs, respectively. After incubation for 6 h, SF(PF127) NPs exhibited stronger yellow overlapping fluorescence than SF NPs, indicating that SF(PF127) NPs could penetrate the mucus layer, but SF NPs lodged within the superficial mucus layer. We further investigated the cellular uptake profiles of SF(PF127) NPs by Calu-3 cells. As shown in Fig. 3B and S3, stronger green fluorescence was observed in Calu-3 cells in the SF(PF127) NPs group than that in the SF NPs group, indicating the enhanced cellular uptake of SF(PF127) NPs. Due to its increased mucus penetration and reduced mucus clearance, SF(PF127) NPs were uptaken more readily by Calu-3 cells. PF127 could decrease NPs affinity to mucus because of its hydrophilic and electronegativity. Therefore, SF(PF127) NPs had a higher mucus penetration ability and Calu-3 cellular uptake aptitude.

3.5. *A549 cellular uptake and Annexin V/PI apoptosis assay*

The A549 cellular uptake of SF(PF127) NPs was viewed by an inverted fluorescence microscope. As shown in Fig. 4A and S4, stronger green fluorescence was detected in A549 cells in the SF(PF127) NPs group than that in the SF NPs group. The results indicated that the coating of PF127 did not hinder the cellular uptake of NPs, but rather enhanced the cellular uptake. Further, we performed flow cytometric analysis to explore the apoptosis-inducing effects of QR-SF NPs and QR-SF(PF127) NPs on A549 cells *in vitro*. According to Fig. 4B, the apoptotic rate of QR-SF NPs and QR-SF(PF127) NPs was 20.81% and 87.88%, respectively. The results showed that the QR-SF(PF127) NPs could induce A549 cells apoptosis

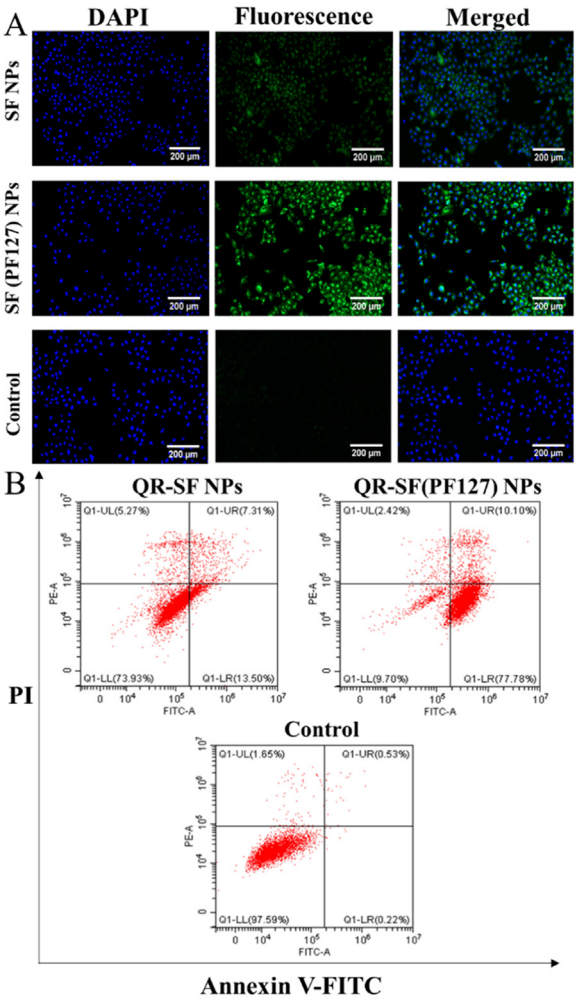

Fig. 4 – (A) *In vitro* cellular uptake studies in A549 cells observed by inverted fluorescence microscope, green and blue colors indicate NPs and DAPI, respectively. Scale bar = 200 μm. (B) The apoptosis-inducing effects of QR-SF NPs and QR-SF(PF127) NPs on A549 cells *in vitro*.

more efficiently than QR-SF NPs, which was consistent with the results of cellular uptake assays, indicating that SF(PF127) nanocarriers could enhance cellular uptake and improve the therapeutic effect of QR in cancer cells.

3.6. *Distribution of NPs in mouse airways*

Mice were dosed *via* nebulization to examine NPs distribution in the mouse airways. Fig. 5 shows the fluorescence distribution of NPs in mice's large airways after intratracheal administration. It was found that the green fluorescence of SF(PF-127) NPs was much stronger than that of SF NPs. Besides, SF(PF-127) NPs with a homogeneous distribution in airways mucus can be observed, while SF NPs presented an uneven distribution. The result indicated that SF(PF-127) NPs have appreciable particle mobility in mucus and good retention in the respiratory tract, which is consistent with the result in Section 3.4. It has been reported that PF127 was effective in attenuating the interaction between

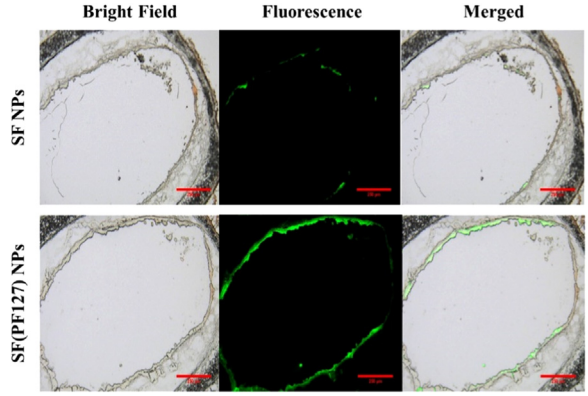

Fig. 5 – Frozen section of tracheas from mice following inhalation administration of coumarin 6-labeled NPs observed by inverted fluorescence microscope. Scale bar =250 μm.

NPs and mucin proteins in the crosslinked network, so the modification of PF-127 on SF NPs could resist the mucociliary clearance.

3.7. In vivo *anti-tumor effect*

To evaluate the therapeutic effect of QR-SF(PF127) NPs *in vivo*, the mice model of melanoma lung metastasis was established. After 14-d pulmonary administration, lungs were extracted to analyze the number of tumor nodules. As shown in Fig. 6A and S7A, pulmonary delivery of QR-SF(PF127) NPs significantly decreased the number of tumor nodules, with 10.6 ± 3.0 tumor nodules in QR-SF(PF127) NPs group. The anti-tumor effect of QR-SF NPs was weaker than QR-SF(PF127) NPs with 24.6 ± 6.5 tumor nodules on average. To further evaluate the anti-tumor effect of NPs, the histopathology of mice lung tissues was determined using H&E staining, and the tumor microvessels density were detected by immunohistochemistry using CD31 staining. As shown in Fig. 6C and S7B, the untreated group exhibited more melanoma tumor and pigmentation, but both treatment groups showed clear relief of melanoma foci. CD31 staining showed that the treatment with QR-SF(PF127) NPs repressed tumoral angiogenesis, microvessel density in the QR-SF(PF127) NPs group was 10 microvessel counts, which was significantly lower than that in the QR-SF NPs group (26 microvessel counts) and the control group (48 microvessel counts), which implied that QR could exert anti-tumor effects by inhibiting microangiogenesis. The TUNEL examining kit was used to detect apoptotic cells in mice lungs, and the results were shown in Fig. 6D and S5. Apparent red fluorescence signals were observed in QR-SF(PF127) NPs group, stronger than the QR-SF NPs group. These results indicated that QR-SF(PF127) NPs considerably facilitated cell apoptosis. Based on the above observations, we speculated that the increased anti-tumor effect of QR was associated with PF127. The surface modification by hydrophilic PF127 facilitates NPs penetration through mucus, improving QR's delivery efficiency and therapeutic effect. Besides, during the 2-week therapy period, all treatment groups appeared no loss

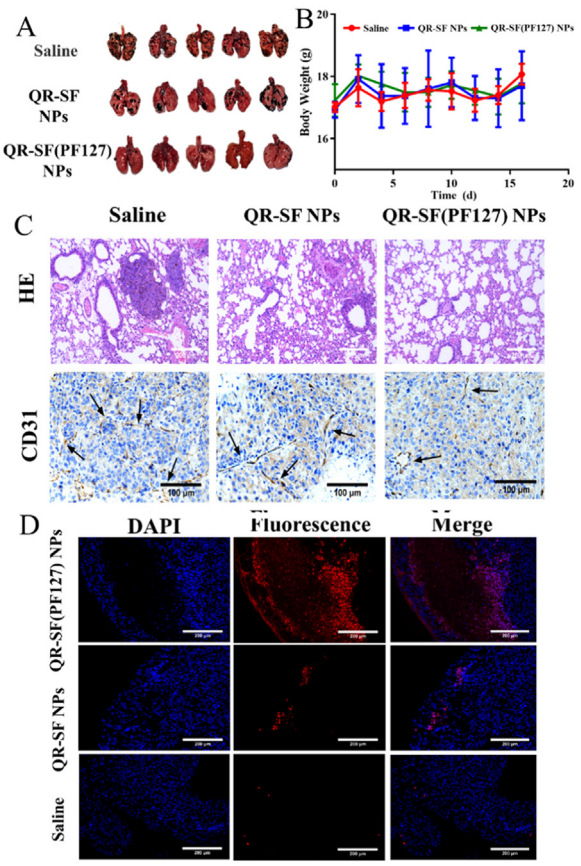

Fig. 6 – (A) Image of QR-loaded NPs inhibiting lung colonization of B16F10 cells. QR was given each day at 5 mg/kg. (B) Mouse body weight curve during treatment. (C) H&E-stained lung tissue slices and CD31-stained blood vessels. Scale bar = 100 μm. (D) The TUNEL assay of tumor tissue sections of SF NPs, SF(PF127) NPs and saline group for the cell apoptosis assay. Scale bar = 200 μm. Each value represents the mean ± SD (n = 5).

of body weight, suggesting the limited side effects of NPs on mice (Fig. 6B). The drug toxicity of each organ was observed by H&E staining (Fig. S6), and there were no obvious pathological changes in each group.

4. Conclusion

In this study, PF127-functionalized silk fibroin (SF) NPs were prepared to explore their capacity for respiratory mucus penetration. The PF127 coating on the SF NPs could attenuate the interaction between NPs and mucin proteins, thus facilitating the diffusion of SF(PF127) NPs in the mucus layer. The QR-SF(PF127) NPs presented an ideal particle size and negative surface charge. Besides, the surface functionalization of PF127 enhanced mucus penetration efficiency of SF NPs. QR-SF(PF127) NPs increased QR's pulmonary delivery efficiency and enhanced its anti-tumor activity *in vivo*. PF127-modified SF NPs may be a promising strategy to attenuate

the interaction with mucin proteins and enhance mucus penetration efficiency in the pulmonary drug delivery system.

Conflicts of interest

The authors declare no conflict of interest.

Acknowledgments

This research was supported by the National Natural Science Foundation of China (No. 52273123); the Graduate Scientific Research and Innovation Foundation of Chongqing, China (No. CYS21072); the Natural Science Foundation of Chongqing (cstc2021jcyj-msxmX0344, cstc2021jcyj-msxmX0342); the Open Research Project from State Key Laboratory of Silkworm GenomeBiology (No. SKLSGB-orp202010).

Supplementary materials

Supplementary material associated with this article can be found, in the online version, at doi:10.1016/j.ajps.2023.100833.

References

[1] Miller M, Hanna N. Advances in systemic therapy for non-small cell lung cancer. BMJ 2021;375:n2363.
[2] Sozzi G, Boeri M, Rossi M, Verri C, Suatoni P, Bravi F, et al. Clinical utility of a plasma-based miRNA signature classifier within computed tomography lung cancer screening: a correlative MILD trial study. J Clin Oncol 2014;32(8):768–73.
[3] Tan XH, Tong L, Li L, Xu JJ, Xie SF, Ji L, et al. Loss of Smad4 promotes aggressive lung cancer metastasis by de-repression of PAK3 via miRNA regulation. Nat Commun 2021;12(1):4853.
[4] Min HY, Lee HY. Mechanisms of resistance to chemotherapy in non-small cell lung cancer. Arch Pharm Res 2021;44(2):146–64.
[5] Lv S, Tang Z, Li M, Lin J, Song W, Liu H, et al. Co-delivery of doxorubicin and paclitaxel by PEG-polypeptide nanovehicle for the treatment of non-small cell lung cancer. Biomaterials 2014;35(23):6118–29.
[6] Sequist LV, Waltman BA, Dias-Santagata D, Digumarthy S, Turke AB, Fidias P, et al. Genotypic and histological evolution of lung cancers acquiring resistance to EGFR inhibitors. Sci Transl Med 2011;3(75):75ra26.
[7] Kumbhar P, Manjappa A, Shah R, Jha NK, Singh SK, Dua K, et al. Inhalation delivery of repurposed drugs for lung cancer: approaches, benefits and challenges. J Control Release 2022;341:1–15.
[8] Ju Y, Cortez-Jugo C, Chen J, Wang TY, Mitchell AJ, Tsantikos E, et al. Engineering of nebulized metal-phenolic capsules for controlled pulmonary deposition. Adv Sci 2020;7(6):1902650.
[9] Mohanraj B, Duan G, Peredo A, Kim M, Tu F, Lee D, et al. Mechanically activated microcapsules for “on-demand” drug delivery in dynamically loaded musculoskeletal tissues. Adv Funct Mater 2019;29(15):1807909.
[10] Dames P, Gleich B, Flemmer A, Hajek K, Seidl N, Wiekhorst F, et al. Targeted delivery of magnetic aerosol droplets to the lung. Nat Nanotechnol 2007;2(8):495–9.
[11] Ahmad J, Akhter S, Rizwanullah M, Amin S, Rahman M, Ahmad MZ, et al. Nanotechnology-based inhalation treatments for lung cancer: state of the art. Nanotechnol Sci Appl 2015;8:55–66.
[12] Elzoghby AO, Hemasa AL, Freag MS. Hybrid protein-inorganic nanoparticles: from tumor-targeted drug delivery to cancer imaging. J Control Release 2016;243:303–22.
[13] Abdelaziz HM, Gaber M, Abd-Elwakil MM, Mabrouk MT, Elgohary MM, Kamel NM, et al. Inhalable particulate drug delivery systems for lung cancer therapy: nanoparticles, microparticles, nanocomposites and nanoaggregates. J Control Release 2018;269:374–92.
[14] Gaber M, Medhat W, Hany M, Saher N, Fang JY, Elzoghby A. Protein-lipid nanohybrids as emerging platforms for drug and gene delivery: challenges and outcomes. J Control Release 2017;254:75–91.
[15] Mehnert W, Mäder K. Solid lipid nanoparticles: production, characterization and applications. Adv Drug Deliv Rev 2001;47(2–3):165–96.
[16] Chana J, Forbes B, Jones SA. Triggered-release nanocapsules for drug delivery to the lungs. Nanomedicine 2015;11(1):89–97.
[17] Zhou QT, Leung SS, Tang P, Parumasivam T, Loh ZH, Chan HK. Inhaled formulations and pulmonary drug delivery systems for respiratory infections. Adv Drug Deliv Rev 2015;85:83–99.
[18] Xu PY, Kankala RK, Pan YJ, Yuan H, Wang SB, Chen AZ. Overcoming multidrug resistance through inhalable siRNA nanoparticles-decorated porous microparticles based on supercritical fluid technology. Int J Nanomedicine 2018;13:4685–98.
[19] Jiménez-López J, El-Hammadi MM, Ortiz R, Cayero-Otero MD, Cabeza L, Perazzoli G, et al. A novel nanoformulation of PLGA with high non-ionic surfactant content improves *in vitro* and *in vivo* PTX activity against lung cancer. Pharmacol Res 2019;141:451–65.
[20] Kim JK, Go EJ, Ko KW, Oh HJ, Han J, Han DK, et al. PLGA microspheres containing hydrophobically modified magnesium hydroxide particles for acid neutralization-mediated anti-inflammation. Tissue Eng Regen Med 2021;18(4):613–22.
[21] Patil HP, Freches D, Karmani L, Duncan GA, Ucakar B, Suk JS, et al. Fate of PEGylated antibody fragments following delivery to the lungs: influence of delivery site, PEG size and lung inflammation. J Control Release 2018;272:62–71.
[22] Mottaghitalab F, Kiani M, Farokhi M, Kundu SC, Reis RL, Gholami M, et al. Targeted delivery system based on gemcitabine-loaded silk fibroin nanoparticles for lung cancer therapy. ACS Appl Mater Interfaces 2017;9(37):31600–11.
[23] Totten JD, Wongpinyochit T, Carrola J, Duarte IF, Seib FP. PEGylation-dependent metabolic rewiring of macrophages with silk fibroin nanoparticles. ACS Appl Mater Interfaces 2019;11(16):14515–25.
[24] Lozano-Pérez AA, Rivero HC, Pérez Hernández MDC, Pagán A, Montalbán MG, Víllora G, et al. Silk fibroin nanoparticles: efficient vehicles for the natural antioxidant quercetin. Int J Pharm 2017;518(1–2):11–19.
[25] Leem JW, Kim MS, Choi SH, Kim SR, Kim SW, Song YM, et al. Edible unclonable functions. Nat Commun 2020;11(1):328.
[26] Liu WP, Zhou ZT, Zhang SQ, Shi ZF, Tabarini J, Lee W, et al. Precise protein photolithography (P-3): high performance biopatterning using silk fibroin light chain as the resist. Adv Sci 2017;4(9):1700191.
[27] Zhao Z, Li Y, Xie MB. Silk Fibroin-based nanoparticles for drug delivery. Int J Mol Sci 2015;16(3):4880–903.
[28] Tian Y, Jiang XJ, Chen X, Shao ZZ, Yang WL. Doxorubicin-loaded magnetic silk fibroin nanoparticles for targeted therapy of multidrug-resistant cancer. Adv Mater 2014;26(43):7393–8.
[29] Lin L, Zhou YX, Quan GL, Pan X, Wu CB. The rough inhalable ciprofloxacin hydrochloride microparticles based on silk fibroin for non-cystic fibrosis bronchiectasis therapy with good biocompatibility. Int J Pharm 2021;607:120974.

[30] Yue PF, Zhou WC, Huang GT, Lei FF, Chen YC, Ma ZL, et al. Nanocrystals based pulmonary inhalation delivery system: advance and challenge. Drug Deliv 2022;29(1):637–51.
[31] Witten J, Samad T, Ribbeck K. Selective permeability of mucus barriers. Curr Opin Biotech 2018;52:124–33.
[32] Abitua PB, Park TJ, Mitchell BJ, Kintner C, Wallingford JB. Dishevelled controls apical docking and planar polarization of basal bodies in ciliated epithelial cells. Dev Biol 2009;331(2):486.
[33] Yuan SP, Hollinger M, Lachowicz-Scroggins ME, Kerr SC, Dunican EM, Daniel BM, et al. Oxidation increases mucin polymer cross-links to stiffen airway mucus gels. Sci Transl Med 2015;7(276):276ra27.
[34] Liu YY, Lv JD, Liu JN, Li M, Xie J, Lv Q, et al. Mucus production stimulated by IFN-AhR signaling triggers hypoxia of COVID-19. Cell Res 2020;30(12):1078–87.
[35] Conte G, Costabile G, Baldassi D, Rondelli V, Bassi R, Colombo D, et al. Hybrid lipid/polymer nanoparticles to tackle the cystic fibrosis mucus barrier in siRNA delivery to the lungs: does PEGylation make the difference? ACS Appl Mater Interfaces 2022;14(6):7565–78.
[36] Huckaby JT, Lai SK. PEGylation for enhancing nanoparticle diffusion in mucus. Adv Drug Deliver Rev 2018;124:125–39.
[37] Yang JD, Duan SZ, Ye H, Ge CL, Piao CX, Chen YB, et al. Pro-peptide-reinforced, mucus-penetrating pulmonary siRNA delivery mitigates cytokine storm in pneumonia. Adv Funct Mater 2021;31(21):2008960.
[38] Bustamante-Marin XM, Ostrowski LE. Cilia and mucociliary clearance. Cold Spring Harb Perspect Biol 2017;9(4):a028241.
[39] Huck BC, Murgia X, Frisch S, Hittinger M, Hidalgo A, Loretz B, et al. Models using native tracheobronchial mucus in the context of pulmonary drug delivery research: composition, structure and barrier properties. Adv Drug Deliver Rev 2022;183:114141.
[40] Zhang XQ, Huang YM, Song HL, Canup BSB, Gou SQ, She ZG, et al. Inhibition of growth and lung metastasis of breast cancer by tumor-homing triple-bioresponsive nanotherapeutics. J Control Release 2020;328:454–69.
[41] Huang YM, Canup BSB, Gou SQ, Chen NX, Dai FY, Xiao B, et al. Oral nanotherapeutics with enhanced mucus penetration and ROS-responsive drug release capacities for delivery of curcumin to colitis tissues. J Mater Chem B 2021;9(6):1604–15.
[42] Pellosi DS, d'Angelo I, Maiolino S, Mitidieri E, d'Emmanuele di Villa Bianca R, Sorrentino R, et al. *In vitro/in vivo* investigation on the potential of Pluronic mixed micelles for pulmonary drug delivery. Eur J Pharm Biopharm 2018;130:30–38.
[43] Hu SS, Yang ZX, Wang S, Wang LP, He QQ, Tang H, et al. Zwitterionic polydopamine modified nanoparticles as an efficient nanoplatform to overcome both the mucus and epithelial barriers. Chem Eng J 2022;428:132107.
[44] Date AA, Halpert G, Babu T, Ortiz J, Kanvinde P, Dimitrion P, et al. Mucus-penetrating budesonide nanosuspension enema for local treatment of inflammatory bowel disease. Biomaterials 2018;185:97–105.
[45] Xu Q, Boylan NJ, Cai S, Miao B, Patel H, Hanes J. Scalable method to produce biodegradable nanoparticles that rapidly penetrate human mucus. J Control Release 2013;170(2):279–286.
[46] Hansson GC. Mucus and mucins in diseases of the intestinal and respiratory tracts. J Intern Med 2019;285(5):479–90.
[47] Li XY, Chen D, Le CY, Zhu CL, Gan Y, Hovgaard L, et al. Novel mucus-penetrating liposomes as a potential oral drug delivery system: preparation, *in vitro* characterization, and enhanced cellular uptake. Int J Nanomed 2011;6:3151–62.
[48] Vinayak M, Maurya AK. Quercetin loaded nanoparticles in targeting cancer: recent development. Anticancer Agents Med Chem 2019;19(13):1560–76.
[49] Ekstrom AM, Serafini M, Nyren O, Wolk A, Bosetti C, Bellocco R. Dietary quercetin intake and risk of gastric cancer: results from a population-based study in Sweden. Ann Oncol 2011;22(2):438–43.
[50] Liu FT, Agrawal SG, Movasaghi Z, Wyatt PB, Rehman IU, Gribben JG, et al. Dietary flavonoids inhibit the anticancer effects of the proteasome inhibitor bortezomib. Blood 2008;112(9):3835–46.